Inorganic Chemistry, 2023, 62, 11, 4625–4636. DOI: **https://doi.org/10.1021/acs.inorgchem.3c00057**

The Highly Adaptive Nature of Group 15 *Tris*(quinolyl) Ligands – Studies with Coinage Metals

Álvaro García-Romero,[a^] *Jessica E. Waters,*[b^] *Rajesh B. Jethwa,*[c] *Andrew D. Bond,*[d] *Annie L. Colebatch,* [e] *Raúl García-Rodríguez,*[a] *Dominic S. Wright*[d*]

a. GIR MIOMeT-IU Cinquima-Química Inorgánica Facultad de Ciencias, Universidad de Valladolid, Campus Miguel Delibes, 47011 Valladolid (Spain), raul.garcia.rodriguez@uva.es

b. The Francis Crick Institute, 1 Midland Road, London NW1 1AT. jessica.waters@crick.ac.uk

c. Institute of Science and Technology Austria (ISTA), Am Campus 1, 3400, Klosterneuburg, Austria.

d. Yusuf Hamied Department of Chemistry, University of Cambridge, Lensfield Road, Cambridge CB2 1EW, UK. dsw1000@cam.ac.uk

e. Research School of Chemistry, The Australian National University, Canberra, ACT 2601. annie.colebatch@anu.edu.au

^ both authors contributed equally to the paper.

KEYWORDS *tris*(quinolyl) ligands, bismuthine, stibine, main-group ligands, coordination

ABSTRACT The substitution of heavier, more metallic atoms into classical organic ligand frameworks provides an important strategy for tuning ligand properties, such as ligand bite and donor character, and is the basis for the emerging area of main-group supramolecular chemistry. In this paper we explore two new ligands [E(2-Me-8-qy)$_3$] [E = Sb (**1**), Bi (**2**); qy = quinolyl], allowing a fundamental comparison of their coordination behavior with classical *tris*(2-pyridyl) ligands of the type [E'(2-py)$_3$] (E = a range of bridgehead atoms and groups, py = pyridyl). A range of new coordination modes to Cu^+, Ag^+ and Au^+ is seen for **1** and **2**, in the absence of steric constraints at the bridgehead and with their more remote N-donor atoms. A particular feature is the adaptive nature of these new ligands, with the ability to adjust coordination mode in response to the hard-soft character of coordinated metal ions, influenced also by the character of the bridgehead atom (Sb or Bi). These features can be seen in a comparison between [Cu$_2${Sb(2-Me-8-qy)$_3$}$_2$](PF$_6$)$_2$ (**1**·CuPF$_6$) and [Cu{Bi(2-Me-8-qy)$_3$}](PF$_6$) (**2**·CuPF$_6$), the first containing a dimeric cation in which **1** adopts an unprecedented intramolecular *N,N,Sb*-coordination mode while in the second **2** adopts an unusual *N,N,(π-)C*-coordination mode. In contrast, the previously reported analogous ligands [E(6-Me-2-py)$_3$] (E = Sb, Bi; 2-py = 2-pyridyl) show a *tris*-chelating mode in their complexes with CuPF$_6$, which is typical for the extensive *tris*(2-pyridyl) family with a range of metals. The greater polarity of the Bi-C bond in **2** results in ligand transfer reactions with Au(I). Although this reactivity is not in itself unusual, the characterization of several products by single-crystal X-ray diffraction provides snapshots of the

ligand-transfer reaction involved, with one of the products (the bimetallic complex [(BiCl){$ClAu_2$(2-Me-8-qy)$_3$}] (**8**)) containing a Au_2Bi core in which the shortest Au→Bi donor-acceptor bond to date is observed.

INTRODUCTION

Tripodal, facially coordinating *tris*(pyridyl) ligands have far-reaching applications in coordination, organometallic, catalysis, and supramolecular chemistry.[1,2] The selection of the bridgehead atom and the position of the N-donor atoms in the pyridyl rings have a fundamental impact on the behavior and coordination properties of this family of ligands.[3,4] Classically, studies have focused on *tris*(2-pyridyl) ligands containing non-metallic bridgehead atoms, E(2-py)$_3$ (e.g., E = CR, COR, CH, N, P, P=O; 2-py = 2-pyridyl).[1] However, incorporating heavier and more metallic main-group bridgehead atoms has been shown to provide an important tool for tuning the ligand character, enabling systematic modification of the bite angle, donor/acceptor properties, and reactivity.[2,5–14] Recent studies have explored the coordination chemistry of *tris*(2-pyridyl) ligands based on Sb and Bi, which coordinate metals (e.g., Cu^+, Ag^+, Li^+) through the three pyridyl arms in a *N,N,N*-chelate coordination mode, which is typical of the *tris*(2-pyridyl) family (intramolecular coordination, Figure 1a).[14,15] In addition, changing the position of the pyridyl N-donor atom from the 2- to the 3-position with respect to the bridgehead atom/group significantly changes the coordination behaviour of the ligands, permitting the coordination of multiple metal centers.[16,17] The coordination of the *tris*(3-pyridyl) and *tris*(4-pyridyl) ligands to Cu and Ag salts gives extended structures involving a combination of N-donor and bridgehead-donor bonding (intermolecular coordination, Figure 1b).[18,19]

Despite increasing interest in this area, the elaboration of this type of ligand using extended N-donor polyaromatic donor groups has been largely ignored as a means of modifying the coordination character. The first example of this type containing a heavier element bridgehead was $MeSi(3\text{-}qy)_3$ (qy = quinolyl),[20–22] while the first example possessing a fully metallic bridgehead atom was only reported recently. In $[\{EtAl(2\text{-}Me\text{-}8\text{-}qy)_3\}Li]$ (containing the anion $[EtAl(2\text{-}Me\text{-}8\text{-}qy)_3]^-$) the Li^+ cation has an unusual trigonal planar, three-coordinate arrangement due to the combination of steric effects and the geometric constraints imposed by the orientation of the donor quinolyl N-atoms (Figure 1c).[23] In the current study we explore the first heavier Group 15 examples of this type of ligand (E = Sb, Bi) (Figure 1d), which combine the flexibility of the 8-quinolyl donor set with ability for lone-pair donation by the metal bridgehead. This produces a remarkably adaptable multidentate ligand arrangement and unique coordination modes in this area, giving intermolecular and intramolecular metal coordination simultaneously.

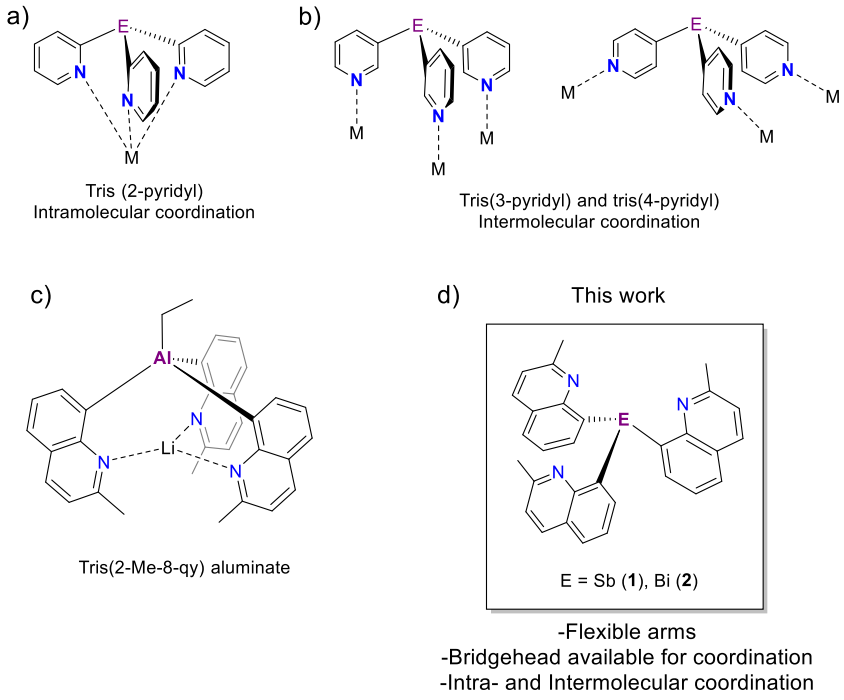

Figure 1. (a) The normal coordination mode seen in previously reported *tris*(2-pyridyl) ligands, (b) The coordination modes for *tris*(3-pyridyl) and *tris*(4-pyridyl) ligands (forming extended arrangements involving *N,N,N*- or *N,N,N,E*- coordination), (c) the structure of [{EtAl(2-Me-8-qy)$_3$}Li], and (d) the new *tris*(2-Me-8-quinolyl) Group 15 ligands introduced in the current study.

RESULTS AND DISCUSSION

Ligand Synthesis

The synthesis of both the new *tris*-quinolyl antimony and bismuth ligands [E(2-Me-8-qy)$_3$] [E = Sb (**1**), Bi (**2**)] is similar to that of the previously reported Al(III) counterpart [EtAl(2-Me-8-qy)$_3$]$^-$ [23] and is achieved *via* the lithium-halogen exchange of 8-bromo-2-methylquinoline with ^{n}BuLi at −78 °C in THF followed by a 3:1 reaction with ECl_3 (Scheme 1). Previous work on the unsubstituted 2-pyridyl Group 15 counterparts indicated that these ligands can decompose through reductive elimination of the 2-pyridyl rings, a problem that appears to be suppressed by using substitution of the ring units at the 6-position (i.e., adjacent to the donor-N atom), possibly providing electronic stabilisation.[14] In order to avoid the possibility of decomposition in this case, the 2-methyl substituted quinolyl ring was used (again with the Me-group adjacent to the donor N-atom).

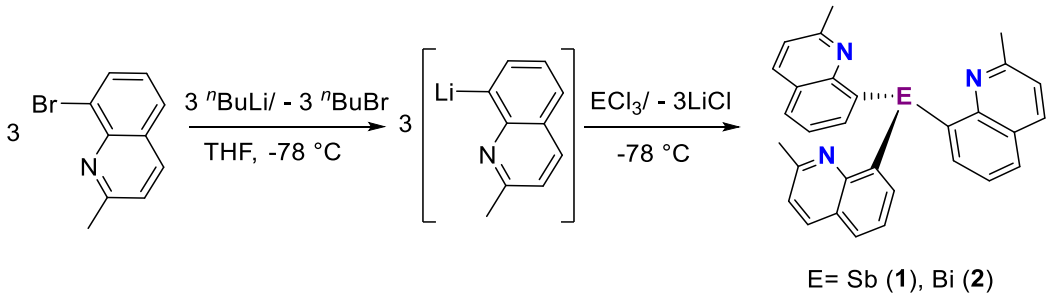

Scheme 1. Synthesis of the ligands Sb(2-Me-8-qy)$_3$ (**1**) and Bi(2-Me-8-qy)$_3$ (**2**).

Recrystallization from dichloromethane (DCM)/*n*-hexane yields both ligands as colorless needle-like crystals (in 41% and 32% yields for **1** and **2**, respectively), without the need for further purification. In addition to X-ray diffraction, compounds **1** and **2** were characterised by NMR spectroscopy, elemental analysis, and mass spectrometry (see SI). Unlike their aluminate counterparts, both ligands are air- and moisture-stable and no hydrolysis was observed for either ligand after six days in deuterated benzene in the presence of water (ca. 2 eq. H_2O). However, as a precaution they are best stored for prolonged periods in solid form under a N_2 atmosphere.

The solid-state structures of compounds **1** and **2** are presented in Figure 2. As expected, they both have pyramidal Sb(III) and Bi(III) centers, with the less obtuse C-Bi-C angles in **2** [C_{py}-Bi-C_{py} range 91.31(9)-92.54(9)°] indicating somewhat more *p*-character in the C-Bi bonds and higher *s*-character in the metal lone pair compared to the Sb derivative **1** [C_{py}-Sb-C_{py} range 93.83(9)-95.62(9)°]. Interestingly, the 2-Me groups and N-atoms of the quinolyl rings in **1** and **2** are oriented "upwards", towards the lone pairs of the Sb and Bi centers, resulting in relatively short E···N contacts [Sb···N range 3.087(2)-3.153(2) Å cf. 3.61 Å for $\sum_{VDW}$(Sb···N);[24] Bi···N range 3.089(2)-3.190(2) Å cf. 3.62 Å for $\sum_{VDW}$(Bi···N)][24] (Figure 2a and b, right). This is similar to the analogous 2-pyridyl ligands E(6-Me-2-py)$_3$. Although it is unclear whether this conformation in **1** and **2** results from weak E···N interactions or for steric reasons (in the solid state), this orientation of the donor N-atoms provides some indication of the preorganization of the ligand arrangements for simultaneous coordination to metal centers using the N-atoms and E-atoms. It can be noted that in the previously explored Al(III) ligand [EtAl(2-Me-8-qy)$_3$]$^-$, this conformation is precluded on steric grounds by the presence of the bridgehead Et-group.[23] The

absence of LiCl/LiBr coordination in **1** and **2** (scavenged from their syntheses) means that there is no further purification required before their application as ligands.

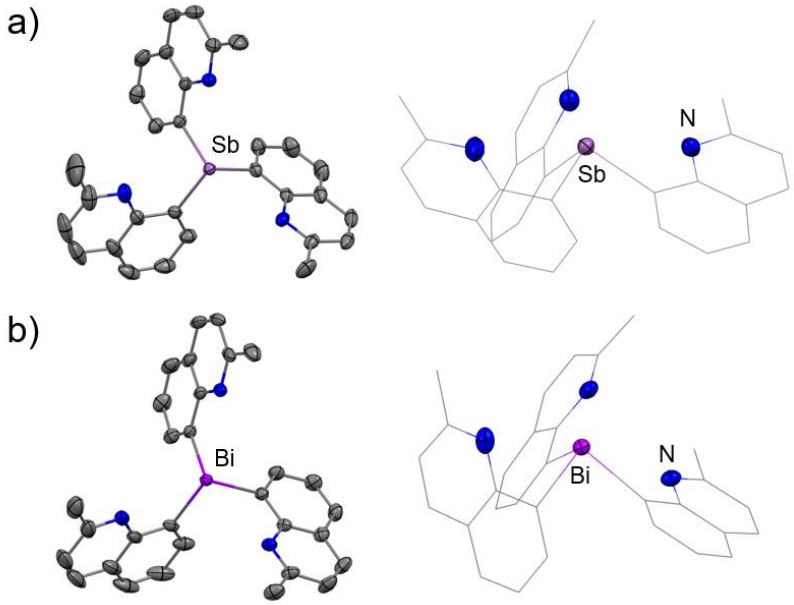

Figure 2. Solid-state structures of (a) **1**, top-view (left) and side-view (right), and (b) **2**, top-view (left) and side-view (right). Displacement ellipsoids shown at 50% probability; H-atoms and a lattice-bound molecule of DCM in compound **1** are omitted for clarity. Selected bond lengths (Å) and angles (°) for **1**: Sb-C_{qy} 2.156(2)-2.169(2); C_{qy}-Sb-C_{qy} 93.83(9)-95.62(9); for **2**: Bi-C_{qy} 2.260(3)-2.265(3), C_{qy}-Bi-C_{qy} 91.31(9)-92.54(9). Color key: C (grey), N (blue), Sb (light purple), Bi (purple).

Coordination Chemistry

With the new ligands **1** and **2** in hand, we next explored their coordination chemistry and reactivity towards coinage metals (Cu^+, Ag^+ and Au^+). The slow diffusion of a solution of

[Cu(MeCN)$_4$]PF$_6$ (1 eq.) in THF into a DCM solution of **1** over 1 week gave crystals of the complex **1**·CuPF$_6$ (in 56% yield) (Scheme 2). In addition to single-crystal X-ray analysis, **1**·CuPF$_6$ was characterised by NMR spectroscopy, elemental analysis, and mass spectrometry (see SI).

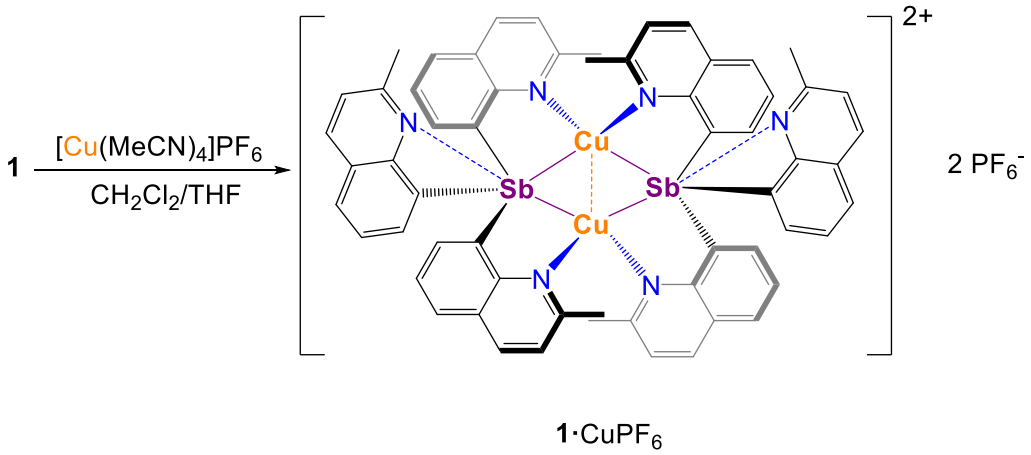

Scheme 2. Synthesis of Cu complex **1**·CuPF$_6$.

The X-ray structure shows that the complex is an ion-separated species [Cu$_2${Sb(2-Me-8-qy)$_3$}$_2$](PF$_6$)$_2$ (**1**·CuPF$_6$) containing a dimeric cation [Cu$_2${Sb(2-Me-8-qy)$_3$}$_2$]$^{2+}$ in which each of the ligands **1** coordinates both of the Cu(I) centers, using two of the quinolyl N-donor atoms and the Sb(III) lone pair simultaneously (Figure 3a). The central rhombic Sb$_2$Cu$_2$ ring unit of the cation is formed by the μ$_2$-bridging of the Sb(III) centers of the two ligands **1** and produces a short Cu···Cu interaction [Cu···Cu 2.566(2) Å, cf. 2.8 Å for $\sum_{VDW}$(Cu···Cu)].[25] The Sb-Cu bond lengths within the Sb$_2$Cu$_2$ core [range 2.5430(19)-2.5984(19) Å] are comparable to the sum of the covalent radii (2.52-2.71 Å for Sb-Cu)[26,27] and are similar to the donor-acceptor bonds found in previously reported stibine-copper complexes, e.g., [Cu(SbPh$_3$)$_4$][ClO$_4$] (2.5721(15)-2.5768(13) Å).[28] This arrangement is supported by the coordination of two quinolyl arms of each

ligand to the two different copper atoms. The remaining qy-group forms an Sb···N contact with the Sb(III) center of its ligand [Sb···N 2.979(11) and 3.019(11) Å, cf. 3.61 Å for $A\sum_{VDW}$(Sb···N)].[24] As a result of this unique μ_2-*Sb,N,N* coordination mode in which **1** acts in a similar way to a pincer ligand, each of the Cu(I) centers is coordinated by two qy-N atoms from different ligands and two Sb(III) bridgehead atoms (Figure 3a). Relevant to the double-bridging of the Sb atom seen in **1**·$CuPF_6$ (and in **1**·$AgSbF_6$, later) is a report of the triple-bridging of the Group 15 bridgehead atoms of the ligand $Pn(C_6H_4P^iPr_2)_3$ in the cage compounds $[Pn(C_6H_4P^iPr_2)_3(MCl)_3]$ (Pn = Sb, Bi; M = Cu, Ag).[29] A further interesting feature of the cation of **1**·$CuPF_6$ is shown in Figure 3b, in which the quinolyl ring units of the two ligand molecules interdigitate, forming an arrangement resembling a "sextuple embrace"[30] (highlighted in red and blue). This presumably reinforces the structural arrangement by additional π-π arene and C-H/π-arene interactions.

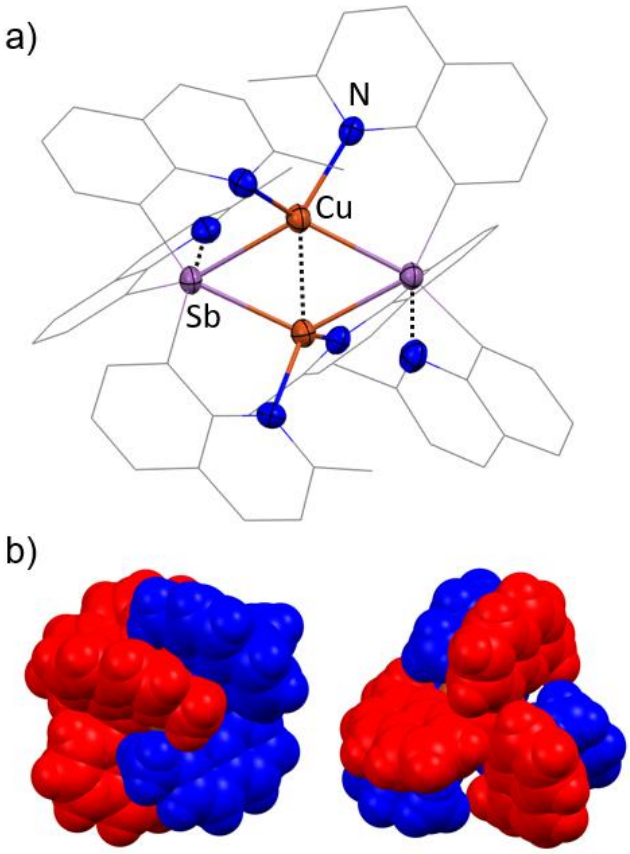

Figure 3. a) Solid-state structure of the dimeric cation of **1**·$CuPF_6$. Displacement ellipsoids shown at 50% probability; H-atoms and the PF_6^- anions are omitted for clarity. b) Side- and top-space filling view of the cation with the two ligand molecules highlighted in red and blue. Selected bond lengths (Å) and angles (°) for **1**·$CuPF_6$: Sb-C_{qy} 2.106(13)-2.154(11); C_{qy}-Sb-C_{qy} 99.0(5)-102.1(5); Sb-Cu 2.5451(19)-2.5884(19); N-Cu 2.072(10)-2.109(10). Color key: C (grey), N (blue), Sb (light purple), Cu (orange).

Although two (Cu-coordinated and uncoordinated) qy-environments are present in the solid-state structure of the cation of **1**·$CuPF_6$, the ^{1}H NMR spectrum shows only one set of qy-resonances in DCM solution at room temperature, presumably due to interchange of the two qy-groups. However, these environments remained unresolved even when the temperature was decreased to

–30 ºC, indicating that either dimers are fluxional with a low activation energy or that dimers dissociate in solution (potentially into monomers).

We next explored the effect of changing to the bismuth ligand **2** on the coordination chemistry with Cu(I). The slow diffusion of *n*-hexane into a DCM solution of **2** with $[Cu(MeCN)_4]PF_6$ over 1 week gave crystals of the complex **2**·$CuPF_6$ (isolated in 55% yield) (Scheme 3). **2**·$CuPF_6$ was characterized using single-crystal X-ray diffraction, NMR spectroscopy, elemental analysis, and mass spectrometry (See SI).

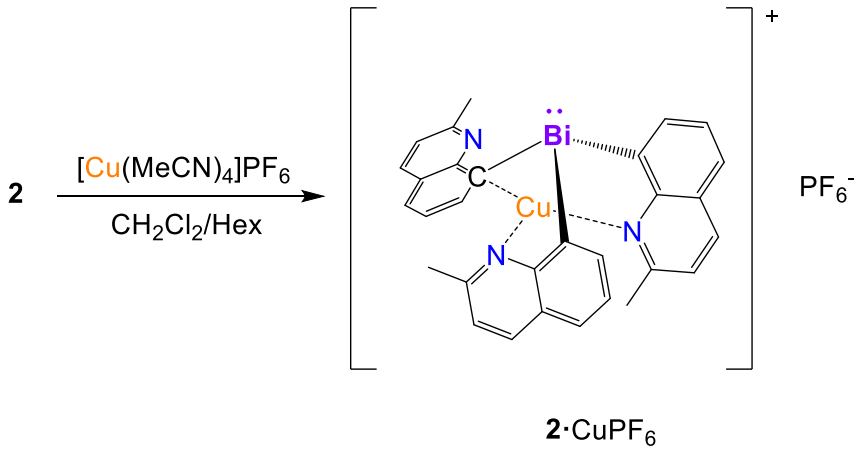

Scheme 3. Synthesis of Cu complex **2**·$CuPF_6$.

In contrast to **1**·$CuPF_6$, the ion-separated structure of complex $[Cu\{Bi(2\text{-Me-8-qy})_3\}](PF_6)$ [**2**·$CuPF_6$] contains a monomeric cation in the solid state (Figure 4), the absence of Bi-Cu bonding (which is integral to the formation of a dimer like **1**·$CuPF_6$) presumably being due to the lower Lewis basicity of the Bi lone pair as a result of its greater *s*-character. The Cu(I) center in the cation of **2**·$CuPF_6$ is coordinated by only two of the three 2-qy N atoms of the ligand **2**, with the third quinolyl groups forming a side-on C···Cu interaction involving the bismuth-bonded C atom [C···Cu 2.253(3) Å, cf. 3.1 Å for $\sum_{VDW}$(C···Cu)].[24,25] The observation of this *N,N,π*-C

coordination mode contrasts with the *N,N,N*-mode seen in the lithium aluminate [{EtAl(2-Me-8-qy)$_3$}Li].[23] This is probably due to the effect of the more acute C-E-C angles at the bridgehead of **2** in the complex (range 98.17(10)-103.18(11)° vs. range 109.2(1)-114.0(1)° for [{EtAl(2-Me-8-qy)$_3$}Li]) and potentially to the slightly larger size of Cu(I) compared to Li^+ (ionic radii 0.73 vs 0.74 Å for Li^+ and Cu^+, respectively),[31] since both would result in strain in the ligand **2** in the case of *N,N,N*-coordination of the ion. This highly unusual *N,N,π-C* coordination mode gives the Cu(I) ion a nearly planar, T-shaped geometry. The closest example to this is seen in [$Mo_2(CO)_6${P(6-Me-2-py)$_3$-μ^2:k^1P;k^3N,N',C,C'}{P(6-Me-2-py)$_3$-k^2P,N}], in which two of the carbon atoms of a P(2-py)$_3$ ligand π-bond to a Mo(0) center (a k^3N,N',C,C'-bonding mode).[32]

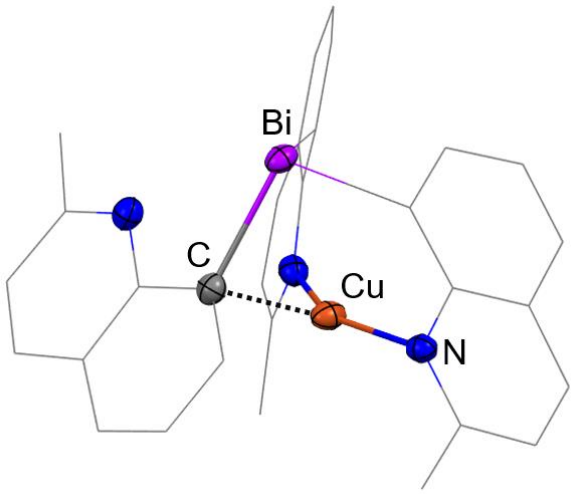

Figure 4. Molecular structure of complex **2**·$CuPF_6$. Displacement ellipsoids shown at 50% probability; H-atoms and the PF_6^- anion are omitted for clarity. Selected bond lengths (Å) and angles (°) for **1**·$CuPF_6$: Bi-C_{qy} 2.283(3)-2.292(3); C_{qy}-Bi-C_{qy} 98.17(10)-103.18(11), N-Cu 1.934(3)-1.938(3), C···Cu 2.253(3), C-Cu-N 102.59(11) and 107.53(10), N-Cu-N 147.77(11). Color key: C (grey), N (blue), Bi (purple), Cu (orange).

As with compound **1**·$CuPF_6$, the two different quinolyl environments (N-coordinated and π-C coordinated) in **2**·$CuPF_6$ are not observed in the ^{1}H NMR spectrum at room temperature and variable-temperature ^{1}H NMR experiments revealed no splitting of the quinolyl resonances down to –30 ºC (See SI).

DFT computational analysis (see Experimental Section, Computational Details) was undertaken on the freely-refined structure of the cation [**2**·Cu]$^+$ (*N,N,π-C* coordination mode) and the hypothetical *N*,*N*,*N*-coordinated analogue (similar to that found in [EtAl(2-Me-8-qy)$_3$}Li][23] and in the *tris*(pyridyl) ligand of [{Bi(6-Me-2-py)$_3$}Cu]PF_6[14]). The results show that the *N,N,π-C* coordination mode provides 7.35 kcal/mol greater stability than the *N*,*N*,*N*-coordination mode (probably largely as a consequence of lower ligand strain). NBO atomic natural charges were calculated for the optimized geometries of **2**, the hypothetical *N*,*N*,*N*-coordinated [**2**·Cu]$^+$ cation, and the experimentally observed [**2**·Cu]$^+$ cation (Figure 5). The solely σ-bonded qy ligands in **2**, *N*,*N*,*N*-coordinated [**2**·Cu]$^+$ and [**2**·Cu]$^+$ have similar polarities, however, the *π-C* coordination in [**2**·Cu]$^+$ results in a large increase in charge on the C-atom involved and far greater C-Bi bond polarity. Specifically, the differences between the atomic charges at the Bi atom and the solely σ-bonded C_{qy} atoms are 1.59 for ligand **2** (Figure 5a), 1.57 (average) for *N*,*N*,*N*-coordinated [**2**·Cu]$^+$ (Figure 5b), and 1.58 in the experimentally observed cation [**2**·Cu]$^+$ (Figure 5c), while there is a large increase to 1.69 for the *π*-C-Cu interaction in the latter (Figure 5c). The development of negative charge on the Bi-bonded carbon atom (C_1) suggests that there is probably a significant ionic contribution to the *π*-C-Bi interaction. In addition, however, from the natural bond order analysis of the [**2**·Cu]$^+$ cation it is apparent that there is also a qy→Cu donor-acceptor interaction between the bonding orbitals of C_1 and C_2, and Cu valence orbitals (Figure 5d), with two components involving sp^2 orbitals and *π*-orbitals of the qy ring (with stabilization

energies of 5.44 and 35.43 kcal/mol, respectively). This is reinforced by a degree of Cu→qy back-donation, with the most significant stabilization component deriving from the Cu *d*-orbitals and the C_1-C_2 π-antibonding orbitals (17.51 kcal/mol).

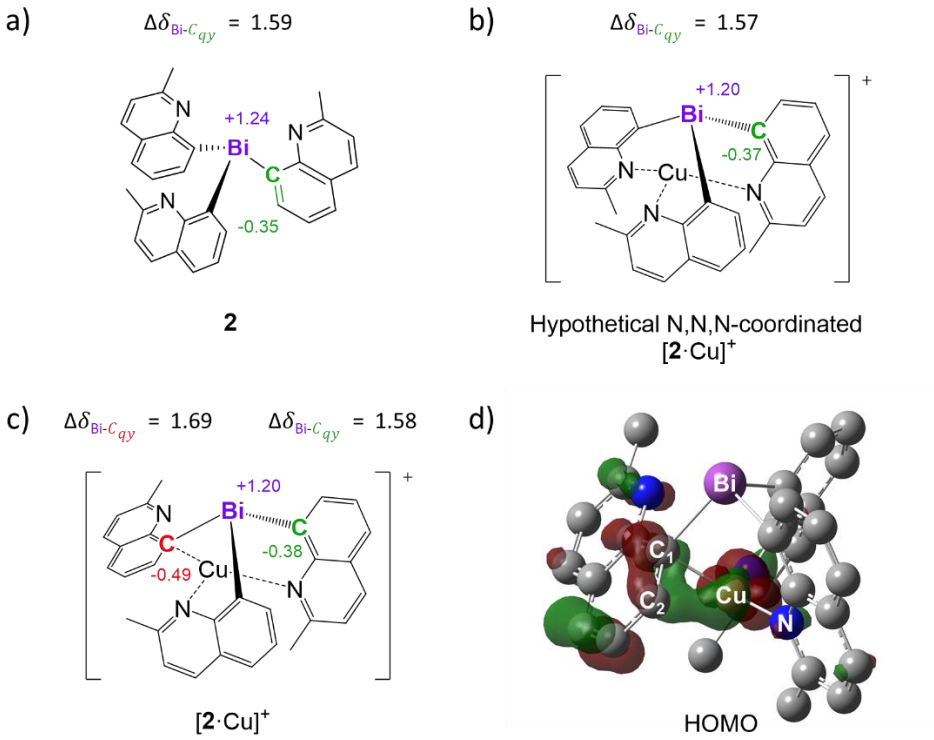

Figure 5. NBO atomic natural charges and Bi-C_{qy} bond polarity comparison between (a) **2**, (b) *N,N,N*-coordinated [**2**·Cu]$^+$ and (c) experimentally observed [**2**·Cu]$^+$, obtained from DFT calculations. The π-C coordination in [**2**·Cu]$^+$ results in a large increase in Bi-C_{qy} bond polarization. (d) Representation of the calculated HOMO of [**2**·Cu]$^+$. The MO isovalues are plotted at 0.045 e/au^3 and H-atoms are omitted for clarity. Color key: C (grey), N (blue), Bi (purple), Cu (orange).

The structures of the copper complexes **1**·$CuPF_6$ and **2**·$CuPF_6$ illustrate the profound effect of the bridgehead atom on the coordination chemistry of the ligands as well as giving a first glimpse of

the highly adaptive nature of the Group 15 *tris*(quinolyl) ligands which makes them significantly different from their *tris*(2-pyridyl) relatives (where *N,N,N*-coordination is the norm).

The slow diffusion of *n*-hexane into a DCM solution of **1** and $AgSbF_6$ at room temperature over 1 week yielded a mixture of colorless needles and colorless blocks which were initially analysed by X-ray diffraction. The colorless needles correspond to the complex **1**·$AgSbF_6$, having a 1:1 stoichiometry of **1** and $AgPF_6$ and a similar dimeric structure to **1**·$CuPF_6$, while the colorless blocks are (**1**)$_2$·$AgSbF_6$**,** in which just one Ag atom is coordinated by two Sb ligands (Scheme 4).

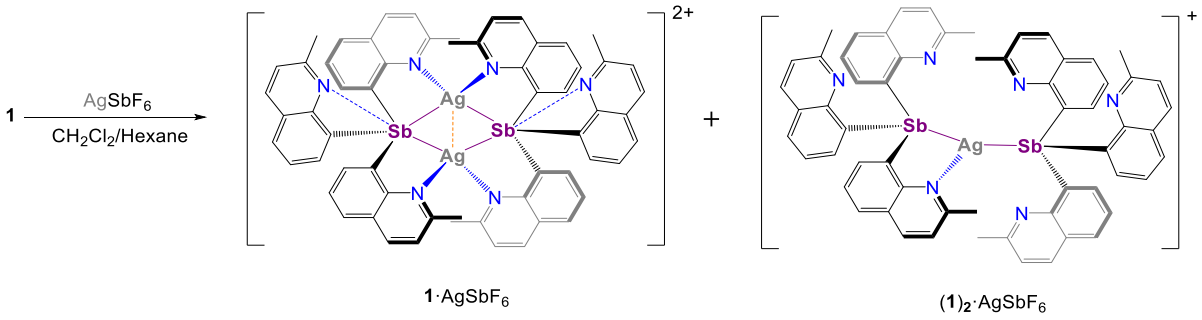

Scheme 4. Synthesis of Ag complexes of **1**·$AgSbF_6$, (**1**)$_2$ $AgSbF_6$. The SbF_6^- anions are omitted for clarity.

The X-ray structures of the cations in **1**·$AgSbF_6$ and (**1**)$_2$·$AgSbF_6$ are shown in Figure 6. The cation of **1**·$AgSbF_6$ has the same dimeric structure as that in **1**·$CuPF_6$, with the each of the Sb centers of the two ligands **1** present bridging the Ag^+ cations and forming a $Ag_2(\mu_2\text{-}Sb)_2$ core with a short Ag···Ag contact which is well below that expected for metal interactions [Ag···Ag range 2.692(11)-2.6994(17) Å, cf. 3.44 Å for $\sum_{VDW}$(Ag···Ag)][25] (Figure 6a). The Sb-Ag bond lengths [range 2.73(2)-2.82(2)] are comparable to the sum of the covalent radii (2.68-2.84 Å)[26,27] and are similar to the donor-acceptor bonds found in stibine-silver complexes like $[Ag(SbPh_3)_4][BrO_3]$ (2.7112(7)-2.7379(7) Å).[33] In the crystal structure, the planar $Ag_2(\mu_2\text{-}Sb)_2$

core of the complex is disordered over three equivalent orientations within the 3-fold symmetric ligand scaffold. This makes interpretation of most of the bond lengths and angle at the Ag and Sb center meaningless. In the cation of $(\mathbf{1})_2 \cdot AgSbF_6$ one of the ligands **1** has a chelating *N,Sb*-coordination mode, while the other is bonded to the Ag^+ cation using only the bridgehead Sb atom (Figure 6b). The Sb-Ag distances [2.6200(6) and 2.6535(6) Å] are slightly shorter than those found in the complex $\mathbf{1} \cdot AgSbF_6$, reflecting the lower coordination number of the Ag^+ centers.

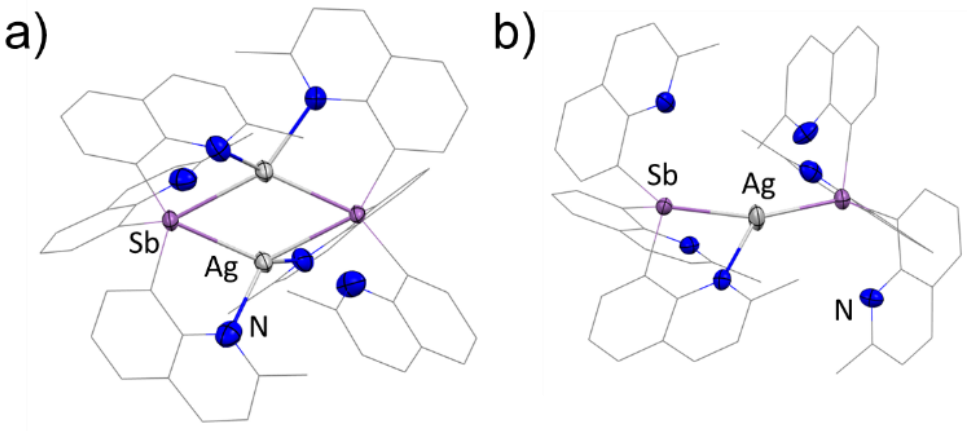

Figure 6. Solid-state structures of (a) the dimeric dication in $\mathbf{1} \cdot AgSbF_6$ and (b) the monocation in $(\mathbf{1})_2 \cdot AgSbF_6$. Displacement ellipsoids shown at 50% probability; H-atoms and the SbF_6^- anions are omitted for clarity. Selected bond lengths (Å) and angles (°) for $\mathbf{1} \cdot AgSbF_6$ (major disorder component for Sb/Ag): Sb-Ag 2.759(5)-2.775(4); Sb-C_{qy} 2.043(19)-2.237(19); Ag-N 2.333(13)-2.433(14); C_{qy}-Sb-C_{qy} 97.8(6)-104.0(7); N-Ag-N 102.0(6)-130.0(4); for $(\mathbf{1})_2 \cdot AgSbF_6$: Sb-$C_{qy}$ 2.119(6)-2.156(6); C_{qy}-Sb-C_{qy} 96.8(2)-102.7(2); Sb-Ag 2.6200(6) and 2.6535(6); Ag-N 2.452(5). Color key: C (grey), N (blue), Sb (light purple), Ag (white).

The structure of the monocation of $(\mathbf{1})_2 \cdot AgSbF_6$ can be regarded as resulting from the extrusion of a Ag^+ cation from the dimeric cation of $\mathbf{1} \cdot AgSbF_6$. Based on this model and the formation of

both complexes in the reaction, the crystalline mixture of **1**·$AgSbF_6$ and (**1**)$_2$·$AgSbF_6$ was investigated further by NMR spectroscopy. The ^{1}H NMR spectrum in DCM at room temperature shows two distinct sets of qy-signals, with a relative ca. 2:1 ratio. The ^{1}H-^{1}H NOESY NMR spectrum reveals the presence of exchange cross-peaks between the two sets of qy-signals. This information, combined with the two different diffusion coefficients of the two sets of qy-signals in the ^{1}H DOSY NMR experiment, suggests that the two different species are in equilibrium (see SI for further information). To obtain further insights into the nature of these species, the dynamic behaviour was evaluated by varying the ligand **1**:$AgSbF_6$ ratio. The aromatic region in the ^{1}H NMR spectrum of the *in situ* reaction of ligand **1** with increasing amounts of $AgSbF_6$ in d_2-DCM is shown in Figure 7 (top). Upon the addition of 0.7 equivalents of $AgSbF_6$ to **1** a shift in the qy-signals is observed, indicative of Ag^+ coordination (the orange signals). The addition of 1 equivalent of $AgSbF_6$ gives a spectrum almost identical to mixture of crystals that obtained from the preparative-scale reaction, with the presence of two sets of signals in ca. 2:1 ratio (orange:blue signals). Finally, the addition of 1.5 eq of $AgSbF_6$ leads to disappearance of the signals marked in orange and increase in intensity of the blue signals. These studies strongly suggest a dynamic equilibrium between **1**·$AgSbF_6$ and (**1**)$_2$·$AgSbF_6$ (Figure 7, bottom). The fact that the resonances marked in blue have a lower diffusion coefficient indicates that these are due to the dication of **1**·$AgSbF_6$, which is also consistent with the appearance of this species at high $AgSbF_6$ concentration (see SI for further information).

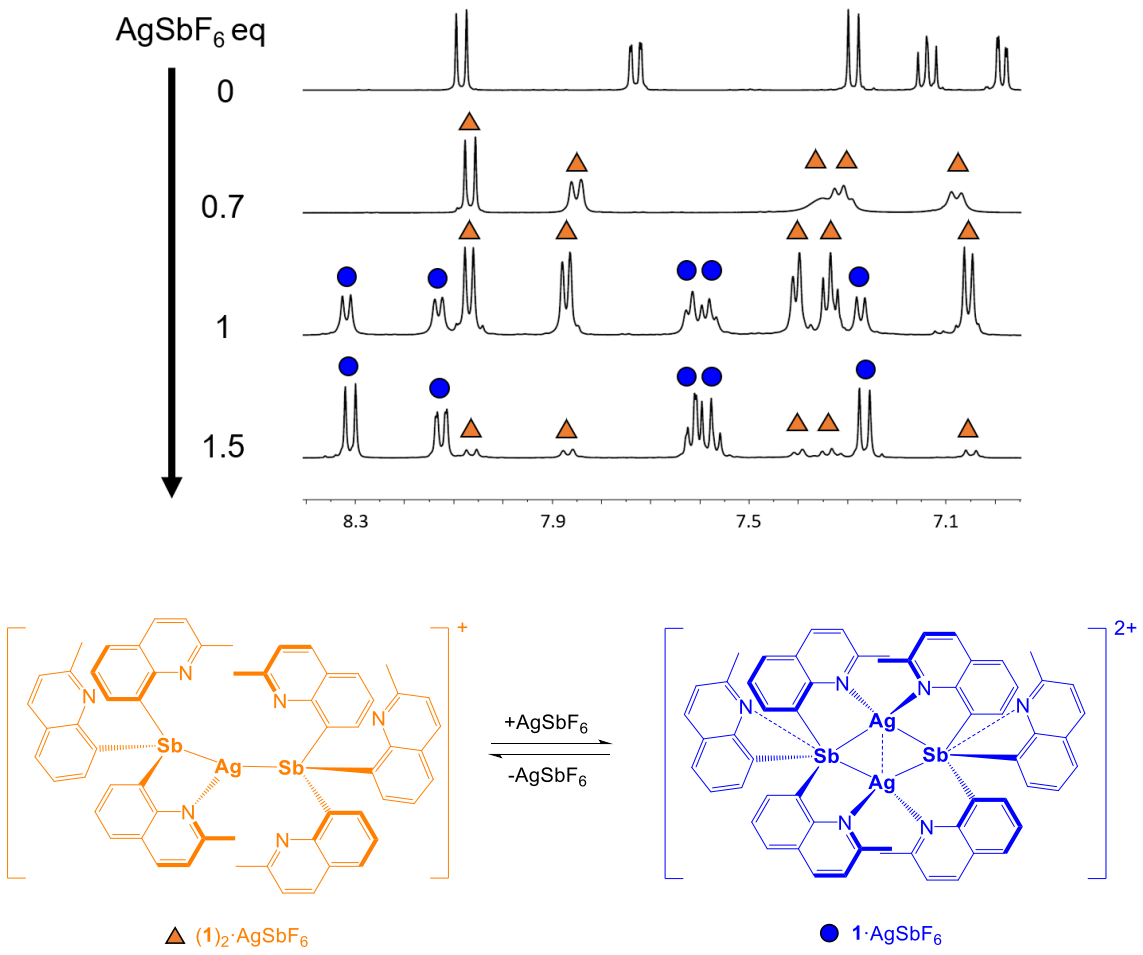

Figure 7. (Top) ^{1}H NMR spectra of the sequential addition of $AgSbF_6$ to a CD_2Cl_2 solution of the free ligand at r.t. (Bottom) Proposed equilibrium between (**1**)$_2$·$AgSbF_6$ and **1**·$AgSbF_6$.

Studies of the coordination of Ag(I) with **2** proved to be unfruitful. For example, the reaction of **2** and $AgSbF_6$ in DCM led to decomposition, and only the hydrolysis product [Ag(2-Me-8-qyH)$_2$]SbF_6 (**3**), along with a grey precipitate which presumably contains metallic Bi and/or Ag, could be isolated (see SI).

In the last part of the current study, we investigated the coordination of Au(I) with ligands **1** and **2**. Slow diffusion of *n*-hexane into a DCM solution of ligand **1** and (THT)AuCl (1 eq.) (THT = tetrahydrothiophene) over a week at –24 ºC gave colorless crystals of [ClAuSb(2-Me-8-qy)$_3$]

(**1**·AuCl) in 64% crystalline yield (Scheme). **1**·AuCl was characterised by X-ray diffraction, NMR spectroscopy, elemental analysis, and mass spectrometry (see SI).

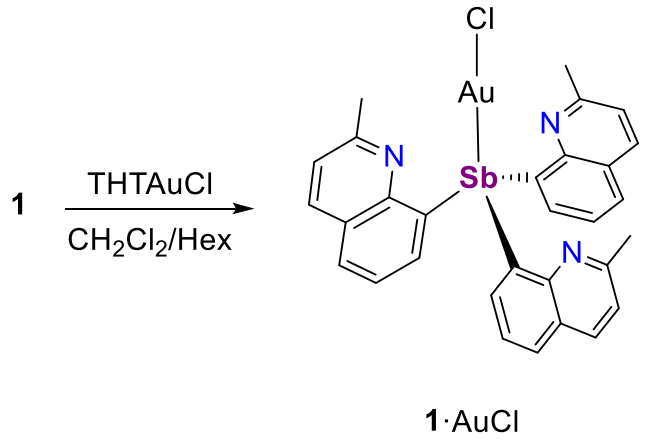

Scheme 5. Synthesis of complex **1**·AuCl.

The solid-state structure of **1**·AuCl (Figure) consists of monomers in which the Sb(III) lone pair forms a donor interaction with Au(I) (2.4842(3) Å; identical within errors to that found for the related monomer $Ph_3SbAuCl$ [2.4818(4) Å]).[34] Presumably the soft Au^+ center suppresses N-coordination by the ligand, thus promoting Sb coordination to the metal atom. The three N-atoms of the quinolyl rings are orientated "upwards" towards the lone pair of the Sb center in a very similar conformation to that seen in the crystal structure of the uncoordinated ligand **1,** with no additional weak interactions to the Au(I) center but potentially retaining the weak Sb···N interactions postulated in **1** itself [Sb-N range 3.005(4)-3.149(4)Å, cf. 3.61Å for $\sum_{VDW}$(Sb···N)][24] (Figure 8).

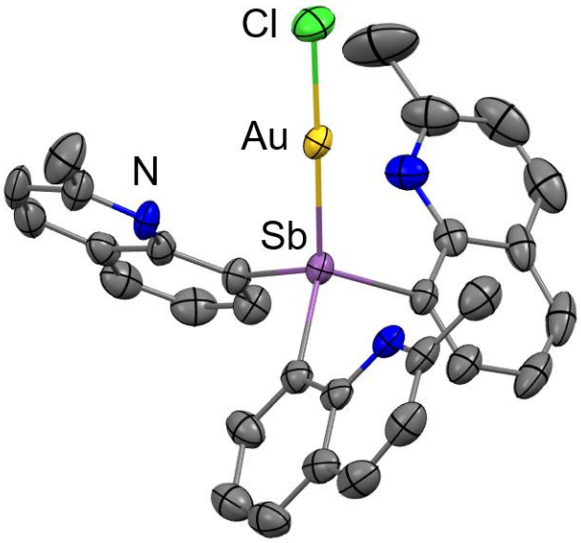

Figure 8. Molecular structure of **1**·AuCl. Displacement ellipsoids shown at 50% probability; H-atoms and one molecule of DCM in the lattice are omitted for clarity. Selected bond lengths (Å) and angles (°) for **1**·AuCl: Sb-C_{qy} 2.122(4)-2.129(4); C_{qy}-Sb-C_{qy} 98.37(17)-100.84(16); Sb-Au 2.4842(3). Color key: C (grey), N (blue), Sb (light purple), Au (yellow), Cl (green).

The NMR-scale reaction of **2** and (THT)AuCl (1:1) in d_2-DCM turned black, and the ^{1}H NMR spectrum showed the formation of several species. After 48 h a dark green solution was formed, along with a gold mirror at the bottom of the NMR tube (see SI). Although the initial formation of the expected 1:1 complex was suggested by high-resolution mass-spectrometry on the reaction mixture, showing the expected [**2**·Au]$^+$ peak at m/z 832.1411 (calcd 832.1440), the isolation of a compound similar to **1**·AuCl was not possible due to its fast decomposition. Despite this, several products were identified by X-ray diffraction from the reaction of ligand **2** and (THT)AuCl (1:1) in DCM on the laboratory scale after layering with *n*-hexane and slow diffusion over three weeks at –24 ºC: [ClBi(2-Me-8-qy)$_2$] (**4**) (colorless thin plates), [Au(2-Me-8-qy)]$_2$ (**5**) (pale green plates), [Au(2-Me-8-qy)]$_4$ (**6**) (red blocks), [{ClBi(2-Me-8-qy)$_2$}$_2${Au$_2$(2-Me-8-qy)$_2$}] (**7**) (yellow blocks), and [(BiCl){ClAu$_2$(2-Me-8-qy)$_3$}] (**8**) (colourless thin plates), along with a

green/black precipitate (presumably containing metallic Bi and/or Au) (Scheme 6). Only the presence of **4** could be confirmed by mass spectrometry [m/z 493.1132 (calcd. 493.1117)]. Since a mixture of **4**-**8** is formed in this reaction, together with metallic decomposition products, meaningful elemental and NMR spectroscopic characterisation of the compounds could not be obtained.

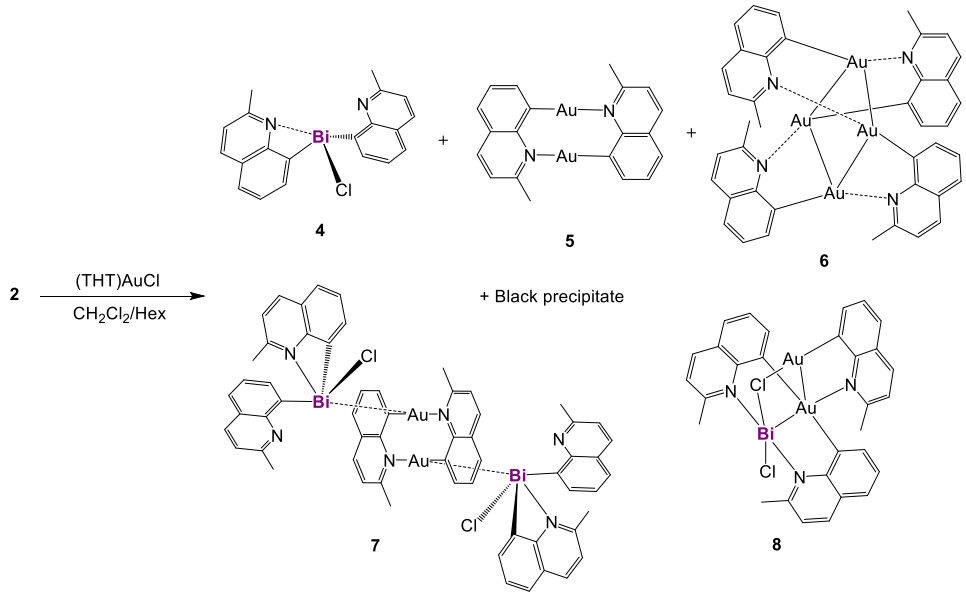

Scheme 6. Reaction of ligand **2** with (THT)AuCl. Single crystals of all five products were picked from the same reaction vessel.

The single-crystal X-ray structures of the complexes **4**, **5**, **6** and **7** are shown in Figure 9. In effect, these species provide snapshots of a reaction sequence that involves qy-ligand transfer from **2** to Au(I), which is the result of the greater polarity of the Bi-C bond of **2** compared to the Sb-C bond **1**. This type of reactivity has been noted in previous reports of Bi(III) *tris*(pyridyl) ligands.[15] The reaction sequence is represented most obviously by the structure of the co-complex **7** in which one of the qy-groups has been transferred to the Au(I) center of AuCl, with displacement of the Cl atom to the Bi(III) atom of **2** giving a unit of **4**. The intermolecular

Au···Bi interactions in **7** (3.5006(4) Å) are shorter than those found in the previously reported salt $[Au(C_6F_5)_2][Bi(C_6H_4CH_2NMe_2\text{-}2)_2]$ (3.7284(5) Å) and are probably largely electrostatic and dispersive in origin.[35] The separate Au and Bi fragments of **7** are seen in the structures of **4**, **5** and **6**, while the structure of **8** (Figure 10) is a unique arrangement that is worthy of individual discussion here (full details of the metric parameters of all the other compounds can be found in the SI, Table S1).

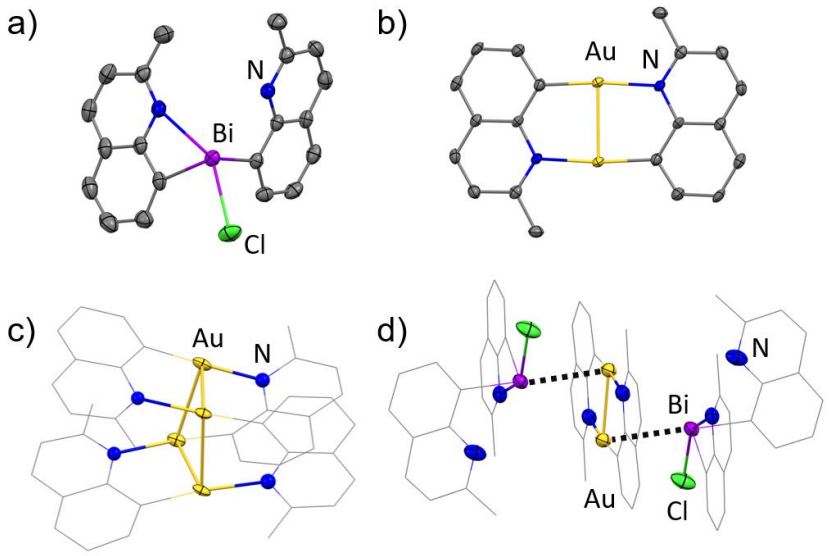

Figure 9. Solid-state structures of a) $[ClBi(2\text{-Me-8-qy})_2]$ (**4**), b) $[Au(2\text{-Me-8-qy})]_2$ (**5**), c) $[Au(2\text{-Me-8-qy})]_4$ (**6**), d) $\{[ClBi(2\text{-Me-8-qy})_2]_2[Au_2(2\text{-Me-8-qy})_2]\}$ (**7**). Displacement ellipsoids shown at 50% probability; H-atoms are omitted for clarity. Color key: C (grey), N (blue), Bi (purple), Cl (green), Au (yellow).

The solid-state structure of **8** is shown in Figure 10a. This can be regarded as being constructed from the association of $(Bi^{III}Cl)^{2+}$, $[ClAu^{I}(2\text{-Me-8-qy})]^{-}$ (Au(1)) and $[Au^{I}(2\text{-Me-8-qy})_2]^{-}$ (Au(2)) subunits. The non-linear Bi(III)–Au(I)-Au(I) metal core of **8** (angle at Au(2) 94.699(10)º) is reinforced by bridging of the Bi-Au and Au···Au bonds by three qy-ligands (Figure 10b). This

gives five-coordinate, approximately square-based pyramidal geometries for the Bi and Au(2) centers, and a T-shaped, three-coordinate arrangement for Au(1). The shortness of the Au(1)···Au(2) distance (2.8320(3) Å) indicates an aurophilic interaction [cf. $\sum_{VDW}$(Au···Au) = 3.32 Å],[25] while the Au(2)···Bi contact [2.5912(3) Å, cf. $\sum_{COV}$(Au-Bi) = 2.75-2.84 Å)][26,27] is the shortest yet observed; shorter even than the unsupported Au-Bi bond (2.659(5) Å) in the cation $[Au(IPr)(ArBi)]^+$ (Ar = *N,C,N*-pincer type ligand, IPr = 1,3-bis(2,6-diisopropylphenyl)imidazolin-2-ylidene).[36] A full analysis of previously reported Au-Bi bonded complexes is provided in the supporting information (Table S3). The shortness of the Au-Bi bond in **8** is presumably due to the bonding of the pincer-like $[Au^{I}(2\text{-Me-8-qy})]_2^-$ ligand in **8** to the highly Lewis acidic Bi(III) atom in the $(Bi^{III}Cl)^{2+}$ fragment. On this basis we assume that this is a Au→Bi donor bond similar to those previously reported by Gabbaï and Limberg.[37–40]

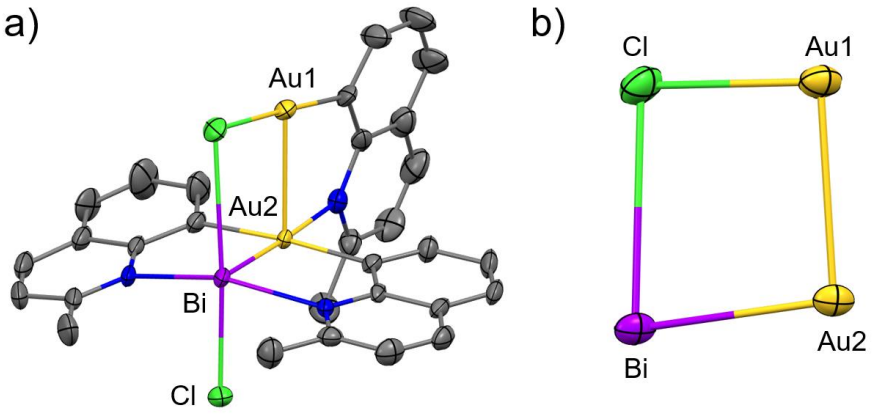

Figure 10. (a) Solid-state structure of the compound $[(BiCl)\{ClAu_2(2\text{-Me-8-qy})_3\}]$ (**8**). Displacement ellipsoids shown at 50% probability; H-atoms are omitted for clarity. Selected bond lengths (Å) and angles (°) for **8**: Bi-N 2.439(4) and 2.459(5); Au(1)-C_{qy} 2.013(6); Au(1)-Cl 2.3611(15); Cl-Au(1)-C_{qy} 177.85(18); Au(2)-C_{qy} 2.128(6) and 2.137(6); C_{qy}-Au(2)-C_{qy} 175.5(2);

Bi-Au(2) 2.5912(3); Bi-Cl 2.5699(14) and 3.1582(16). Color key: C (grey), N (blue), Bi (purple), Cl (green), Au (yellow). (b) The core structure of **8**.

CONCLUSIONS

The results reported here show that in the absence of a bridgehead substituent (like the Et group in the Al(III) anion $[EtAl(2\text{-Me-}8\text{-qy})_3]^-$), *tris*(quinolyl) ligands containing heavier Group 15 bridgeheads can adopt a greater range of coordination modes, because of the absence of large steric congestion in the vicinity of the bridgehead atom. This means that the donor N-atoms and the lone-pair on the bridgehead atom can coordinate metal ions simultaneously (intra- rather than inter-molecular). An initial indication of this is seen in the crystal structures of the Sb ligand **1** and **2** themselves, in which the donor-N atoms are predisposed for cooperative coordination, and is exemplified by the comparable dimeric arrangements of the dications of the Cu(I) and Ag(I) complexes **1**·$CuPF_6$ and **1**·$AgSbF_6$ in which an unprecedented bonding mode involving intramolecular *N,N,Sb*-metal coordination is observed. The ability of these ligands to adapt is seen in the cation of the Cu(I) complex **2**·$CuPF_6$, in which the lower Lewis basicity of the Bi center in **2** (having significantly more *s*-character than the Sb lone pair in **1**) results in a switch to an unusual *N,N,(π-)C*-coordination mode. The softer character of Au(I) underlies the prevalence for Sb-Au bonding in the Au(I) complex **1**·AuCl, while the greater polarity of Bi-C bonds in **2** is responsible for the prominence of qy-ligand transfer in its reaction with (THT)AuCl. Interestingly, crystallographic characterisation of the range of products generated in this case provides snapshots of the nucleophilic exchange reaction occurring, with complex $[(BiCl)\{ClAu_2(2\text{-Me-}8\text{-qy})_3\}]$ (**8**) having an unprecedented arrangement in which a particularly short Au→Bi bond is observed. Our studies are continuing with the exploration of the effects of

altering the N-atom position in the qy-ligand framework, to explore the potential for other types of bonding modes and for supramolecular assembly into MOF-type arrangements.

EXPERIMENTAL SECTION

General Experimental Methods

Syntheses were carried out on a Schlenk line under a nitrogen atmosphere using oven-dried glassware, unless otherwise specified. Starting materials were commercially obtained from suppliers and used as received. Lower temperatures in syntheses were achieved using dry ice/acetone (−78 °C) baths. MeCN and DCM were dried over CaH_2 and distilled under nitrogen. THF and *n*-hexanes were dried over Na/benzophenone and distilled under nitrogen. Deuterated solvents were distilled and/or dried over molecular sieves before use. A nitrogen-filled glove box (Saffron type α) was used to manipulate solids, including room temperature reactions, product recovery and sample preparation for analysis. Yields are given as isolated yields of solid or crystalline products. Room temperature ^{1}H and $^{13}C\{^{1}H\}$ spectra were recorded on a Bruker 400 MHz Avance III HD Smart Probe spectrometer and referenced to the residual solvent peaks. Unambiguous assignments of NMR resonances were made on the basis of 2D NMR experiments (^{1}H-^{1}H COSY, ^{1}H-^{13}C HSQC, ^{1}H-^{13}C HMBC and ^{1}H-^{13}C HMQC). Mass spectra were obtained by positive ion electrospray ionisation using a Thermo Fisher Orbitrap mass spectrometer. Elemental analysis for carbon, hydrogen and nitrogen were performed using a PerkinElmer 240 Elemental Analyser. X-ray data were collected on a Bruker D8-QUEST diffractometer, equipped with an Incoatec IμS Cu microsource (λ = 1.5418 Å) and a PHOTON-III detector operating in shutterless mode. Crystals were mounted on a MiTeGen crystal mount using inert polyfluoroether oil and the analysis was carried out under an Oxford Cryosystems open-flow N_2

Cryostream operating at either 180(2) or 220(2) K. Details of structure solution and refinement are provided in the SI. Data have been deposited at the Cambridge Crystallographic Data Centre, deposition numbers CCDC 2232344-2232356.

Computational Details

All computations were carried out using the Gaussian16 package,[41] in which the hybrid method of Austin, Petersson and Frisch with spherical atom dispersion terms (APFD) was applied.[42] The cc-pvtz-pp basis set was used for the Cu and Bi atoms,[43–46] as found in the EMSL basis set exchange Web site,[47–49] and the 6-31G(d,p) basis set was used for the rest of the atoms. Geometry optimizations were performed without symmetry restrictions using the initial coordinates derived from X-ray data when available, and frequency analyses were performed to ensure that a minimum structure with no imaginary frequencies was achieved in each case. The visualization of the calculation results was performed with GaussView 6.1.[50] The atomic charges resulting from natural population analysis were calculated using the program NBO 7.0[51] for **2** and [**2**·Cu]$^+$. The Bi–C_{qy} bond polarization was calculated as the difference in their atomic charges.

Synthesis

Synthesis of 1. A solution of 8-bromo-2-methylquinoline (666 mg, 3.00 mmol) in THF (10 mL) was cooled to −78 °C. ^{n}BuLi (1.6 M in hexanes, 2.0 mL, 3.2 mmol) was added dropwise, and the red solution was stirred at −78 °C for 1 hour. $SbCl_3$ (228 mg, 1 mmol) in THF (4 mL) was added, resulting in a yellow solution. The solution was allowed to warm to room temperature and stirred overnight. The volatiles were removed under vacuum. The residue was extracted with DCM (20 mL), filtered through Celite and washed through with an extra 20 mL DCM. The solution was

concentrated under vacuum to 20 mL, and hexane (40 mL) was added. Storage for a week at -24 °C yielded **1** as colorless needles. Yield 223 mg. 0.40 mmol, 41%. ^{1}H NMR (298 K, C_6D_6, 400 MHz): δ = 7.54 (m, 3H, H_4+H_8), 7.41 (d, J = 7.3 Hz, 3H, H_6), 6.95 (t, J = 7.3 Hz, 3H, H_5), 6.70 (d, J = 8.4 Hz, 3H, H_9), 2.28 (s, 9H, H_{11} Me). ^{1}H NMR (298 K, CD_2Cl_2, 400 MHz): δ = 8.13 (d, J = 8.4 Hz, 3H, H_8), 7.77 (d, J = 8.0 Hz, 3H, H_6), 7.33 (d, J = 8.4 Hz, 3H, H_9), 7.18 (t, J = 8.0 Hz, 3H, H_5), 7.01 (d, J = 8.0 Hz, H_4), 2.62 (s, 9H, H_{11} Me). ^{13}C{^{1}H} NMR (298 K, C_6D_6, 100.6 MHz): δ = 158.08 (C_{10}), 152.76 (C_2), 146.19 (C_3), 138.38 (C_4), 136.17 (C_8), 127.48 (C_6), 126.76 (C_5), 126.39 (C_7), 121.75 (C_9), 25.02 (C_{11}). ^{13}C{^{1}H} NMR (298 K, CD_2Cl_2, 100.6 MHz): δ = 158.56 (C_{10}), 152.38 (C_2), 144.08 (C_3), 138.13 (C_4), 136.76 (C_8), 127.90 (C_6), 126.70 (C_5), 126.57 (C_7), 122.31 (C_9), 25.43 (C_{11}). ESI-MS(+) (m/z): Found: 548.1084. Calc. for $C_{30}H_{25}N_3Sb$ $[M+H]^+$: 548.1087 (0.5 ppm error). Elemental analysis (%): calcd. for $C_{30}H_{24}N_3Sb$ C 65.7, H 4.4, N 7.7; found: C 65.8, H 4.5, N 7.6.

Synthesis of 2. A solution of 8-bromo-2-methylquinoline (666 mg, 3.00 mmol) in THF (10 mL) was cooled to −78 °C. nBuLi (1.6 M in hexanes, 2.0 mL, 3.2 mmol) was added dropwise, and the red solution was stirred at −78 °C for 1 hour. $BiCl_3$ (315 mg, 1 mmol) in THF (4 mL) was added, resulting in a yellow solution. The solution was allowed to warm to room temperature and stirred overnight. The volatiles were removed under vacuum. The residue was extracted with DCM (20 mL), filtered through Celite and washed through with an extra 20 mL DCM. The solution was concentrated under vacuum to 20 mL, and hexane (40 mL) was added. Storage for a week at -24 °C yielded **2** as colorless blocks. Yield 205 mg. 0.31 mmol, 32%. ^{1}H NMR (298 K, C_6D_6, 400 MHz): δ = 8.21 (d, J = 7.5 Hz, 3H, H_4), 7.59 (d, J = 8.4 Hz, 3H, H_8), 7.47 (d, J = 7.5 Hz, 3H, H_6), 7.04 (t, J = 7.5 Hz, 3H, H_5), 6.70 (d, J = 8.4 Hz, 3H, H_9), 2.29 (s, 9H, H_{11} Me). ^{1}H NMR (298 K, CD_2Cl_2, 400 MHz): δ = 8.12 (d, J = 8.4 Hz, 3H, H_8), 7.76 (d, J = 8.0 Hz, 3H, H_6), 7.65 (d, J = 8.0

Hz, 3H, H_4), 7.27 (d, J = 8.4 Hz, 3H, H_9), 7.21 (t, J = 8.0 Hz, 3H, H_5), 2.60 (s, 9H, H_{11} Me). $^{13}C\{^1H\}$ NMR (298 K, C_6D_6, 100.6 MHz): δ = 162.60 (C_3),158.78 (C_{10}), 153.15 (C_2), 140.54 (C_4), 136.41 (C_8), 129.05 (C_5), 127.23 (C_7), 126.72 (C_6), 121.60 (C_9), 25.16 (C_{11}). $^{13}C\{^1H\}$ NMR (298 K, CD_2Cl_2, 100.6 MHz): δ = 161.80 (C_3), 158.32 (C_{10}), 152.81 (C_2), 140.18 (C_4), 136.93 (C_8), 128.99 (C_5), 127.34 (C_7), 127.04 (C_6), 122.15 (C_9), 25.56 (C_{11}). ESI-MS(+) (m/z): Found: 652.1807. Calc. for $C_{30}H_{25}N_3OBi$ $[M+OH]^+$: 652.1801 (0.9 ppm error). Elemental analysis (%): calcd. for $C_{30}H_{24}N_3Bi$ C 56.7, H 3.8, N 6.6; found: C 56.7, H 3.8, N 6.5.

Synthesis of 1·$CuPF_6$. A solution of **1** (30 mg, 0.054 mmol) in dry DCM (3 mL) was prepared in a narrow Schlenk flask under a N_2 atmosphere. A layer of THF (3 mL) was layered on top of the ligand solution, and a solution of $[Cu(MeCN)_4]PF_6$ (20.4 mg, 0.054 mmol) in THF (3 mL) was then layered carefully on top of the THF layer. The three layers were left to diffuse slowly at room temperature for 1 week, resulting in yellow needles of **1**·$CuPF_6$ suitable for X-ray crystallography. Yield calculated as $\{Cu_2[Sb(2\text{-Me-10-qy})_3]_2\}(PF_6)_2$ 22.7 mg (0.015 mmol, 56%). ^1H NMR (298 K, CD_2Cl_2, 400 MHz): δ = 8.27 (d, J = 8.4 Hz, 3H, H_8), 8.13 (d, J = 7.5 Hz, 3H, H_6), 8.00 (m, 6H, H_4+H_5), 7.13 (d, J = 7.5 Hz, 3H, H_9), 1.87 (s, 9H, H_{11} Me). $^{13}C\{^1H\}$ NMR (298 K, CD_2Cl_2, 100.6 MHz): δ = 162.19 (C_{10}), 149.63 (C_2), 140.01 (C_4+C_8), 132.40 (C_6), 131.68 (C_3), 128.54 (C_7), 128.36 (C_5), 124.37 (C_9), 26.98 (C_{11}). ^{19}F NMR (298 K, CD_2Cl_2, 376.5 MHz): δ = -73.32 (d, J_{PF} = 710 Hz). ^{31}P NMR (298 K, CD_2Cl_2, 162 MHz): δ = -144.52 (sept, J_{PF} = 710 Hz). ESI-MS(+) (m/z): Found: 610.0305. Calc. for $C_{30}H_{24}N_3CuSb$ $[CuSb(2\text{-Me-8-qy})_3]^+$: 610.0304 (0.2 ppm error). Elemental analysis (%): calcd. for $C_{30}H_{24}N_3SbCuF_6P$; C 47.6, H 3.2, N 5.5; found: C 47.3, H 3.3, N 5.4.

Synthesis of 2·$CuPF_6$. A Schlenk tube was charged with **2** (30 mg, 0.047 mmol) and $[Cu(MeCN)_4]PF_6$ (17.6 mg, 0.047 mmol), and 10 mL of DCM was then added. The resulting yellow solution was stirred for 15 mins at room temperature. The solution was filtered with a syringe filter into a narrow Schlenk flask under a N_2 atmosphere, and slow diffusion of *n*-hexane (20 ml) at room temperature yielded **2**·$CuPF_6$ as yellow needles suitable for X-ray crystallography after 1 week. Yield 21.9 mg (0.026 mmol, 55%). ^{1}H NMR (298 K, CD_2Cl_2, 400 MHz): δ = 8.52 (d, J = 7 Hz, 3H, H_4), 8.27 (d, J = 8.3 Hz, 3H, H_8), 8.00 (d, J = 7 Hz, 3H, H_6), 7.72 (t, J = 7 Hz, 3H, H_5), 7.26 (d, J = 8.3 Hz, 3H, H_9), 2.10 (s, 9H, H_{11} Me). ^{13}C{^{1}H} NMR (298 K, CD_2Cl_2, 100.6 MHz): δ = 159.54 (C_{10}), 155.40 (C_3), 152.15 (C_2), 140.13 (C_4+C_8), 130.57 (C_6), 128.98 (C_5), 128.77 (C_7), 123.28 (C_9), 26.19 (C_{11}). ^{19}F NMR (298 K, CD_2Cl_2, 376.5 MHz): δ = -73.48 (d, J_{PF} = 710 Hz). ^{31}P NMR (298 K, CD_2Cl_2, 162 MHz): δ = -144.50 (sep, J_{PF} = 710 Hz). ESI-MS(+) (m/z): Found: 698.1072. Calc. for $C_{30}H_{24}N_3CuBi$ [**2**·Cu]$^+$: 698.1070 (0.3 ppm error). Elemental analysis (%): calcd. for $C_{30}H_{24}N_3BiCuF_6P$; C 42.7, H 2.9, N 5.0; found: C 42.2, H 2.7, N 4.9.

Synthesis of 1·$AgSbF_6$ and (1)$_2$·$AgSbF_6$. A Schlenk tube was charged with **1** (30 mg, 0.054 mmol) and $AgSbF_6$ (18.8 mg, 0.054 mmol), and 10 mL of DCM was then added. The resulting yellow solution was stirred for 15 mins at room temperature. The solution was filtered with a syringe filter into a narrow Schlenk flask under a N_2 atmosphere. Slow diffusion of hexane (10 mL) at room temperature yielded a mixture of **1**·$AgSbF_6$ and (**1**)$_2$·$AgSbF_6$ as colorless needles and colorless blocks, respectively, suitable for X-ray crystallography after 1 week. The crystalline mixture (23 mg) could not be separated manually, and ^{1}H NMR studies showed that **1**·$AgSbF_6$ and (**1**)$_2$·$AgSbF_6$ were present in a 1:2 ratio, respectively. (**1**)$_2$·$AgSbF_6$: ^{1}H NMR (298 K, CD_2Cl_2, 400 MHz): δ = 8.06 (d, J = 8.4 Hz, 3H, H_8), 7.86 (d, J = 7.4 Hz, 3H, H_6), 7.39 (d, J =

7.4 Hz, 3H, H_4), 7.33 (t, J = 7.4 Hz, 3H, H_5), 7.05 (d, J = 8.4 Hz, 3H, H_9), 1.97 (s, 9H, H_{11} Me). **1**·$AgSbF_6$: ^{1}H NMR (298 K, CD_2Cl_2, 400 MHz): δ = 8.31 (d, J = 8.4 Hz, 3H, H_8), 8.11 (d, J = 7.9 Hz, 3H, H_6), 7.6 (m, 3H, H_4 + H_5), 7.26 (d, J = 8.4 Hz, 3H, H_9), 1.95 (s, 9H, H_{11} Me). (**1**)$_2$·$AgSbF_6$: $^{13}C\{^1H\}$ NMR (298 K, CD_2Cl_2, 100.6 MHz): δ = 159.46 (C_{10}), 150.92 (C_2), 138.65 (C_4), 137.71 (C_3), 137.60 (C_8), 129.83 (C_6), 127.06 (C_5+C_7), 122.83 (C_9), 26.01 (C_{11}). **1**·$AgSbF_6$: $^{13}C\{^1H\}$ NMR (298 K, CD_2Cl_2, 100.6 MHz): δ = 161.41 (C_{10}), 149.73 (C_2), 140.48 (C_8), 140.23 (C_4), 132.54 (C_6), 131.31 (C_3), 128.58 (C_7), 128.16 (C_5), 124.04 (C9), 27.68 (C_{11}). ^{19}F NMR (298 K, CD_2Cl_2, 376.5 MHz): δ = -124.4 (m, SbF_6^-). ESI-MS(+) (m/z): Found: 654.0057. Calc. for $C_{30}H_{24}N_3SbAg$ [AgSb(2-Me-8qy)$_3$]$^+$: 698.1070 (0.3 ppm error).

Synthesis of 1·AuCl. A Schlenk tube was charged with **1** (30 mg, 0.054 mmol) and THTAuCl (17.5 mg, 0.047 mmol), and 4 ml of DCM was then added. The resulting colorless solution was stirred for 5 mins at room temperature. The solution was filtered with a syringe filter into a narrow Schlenk flask under a N_2 atmosphere, and slow diffusion of hexane (15 ml) at -24 °C yielded **1**·AuCl as colorless crystals suitable for X-ray crystallography after 1 week, which were dried under vacuum. Yield 28 mg (0.036 mmol, 64%). ^{1}H NMR (298 K, CD_2Cl_2, 400 MHz): δ = 8.11 (d, J = 8.4 Hz, 3H, H_8), 7.90 (d, J = 8.0 Hz, 3H, H_6), 7.54 (d, J = 8.0 Hz, 3H, H_4), 7.36 (t, J = 8.0 Hz, 3H, H_5), 7.29 (d, J = 8.4 Hz, 3H, H_9), 2.46 (s, 9H, H_{11} Me). $^{13}C\{^1H\}$ NMR (298 K, CD_2Cl_2, 100.6 MHz): δ = 159.63 (C_{10}), 150.40 (C_2), 138.05 (C_4), 136.71 (C_8), 135.88 (C_3), 130.16 (C_6), 126.98 (C_7), 126.69 (C_5), 123.19 (C_9), 24.78 (C_{11}). ESI-MS(+) (m/z): Found: 744.0683. Calc. for $C_{30}H_{24}N_3AuSb$ [**1**·Au]$^+$: 744.0674 (1.2 ppm error). Elemental analysis (%): calcd. for $C_{30}H_{24}N_3SbAuCl$ (**1**·AuCl); C 46.1, H 3.1, N 5.4; found: C 46.5, H 3.3, N 5.1.

ASSOCIATED CONTENT

Supporting Information.

The following files are available free of charge: NMR spectra, mass spectra, additional X-ray structures, details and information, and xyz coordinates of DFT optimised structures (PDF).

AUTHOR INFORMATION

Corresponding Author

Prof. Dominic S. Wright, dsw1000@cam.ac.uk

Authors

Author Contributions

A.G.-R., J.E.W. and A.L.C. performed the synthetic studies. R.B.J. and A.G.-R. performed the DFT calculations. A.D.B. collected and solved the crystallographic data. A.L.C., R.G.-R. and D.S.W. supervised the studies. A.G.-R. and D.S.W. wrote the paper. All authors contributed to proof reading and corrections during writing.

Notes

The authors declare no competing financial or other conflicts of interest.

ACKNOWLEDGMENTS

We thank The Walters-Kundert Studentship of Selwyn College (scholarship for J.E.W), The Leverhulme Trust (R.G.-R. and D.S.W, grant RPG-2017-146), the Australian Research Council (A.L.C., DE200100450), the Spanish Ministry of Science and Innovation (MCI) and the Spanish Ministry of Science, Innovation and Universities (MCIU) (R.G.-R., PID2021-124691NB-I00, funded by MCIN/AEI/10.13039/501100011033/FEDER, UE and PGC2018-096880-A-I00,

MCIU/AEI/FEDER), The University of Valladolid and Santander Bank (Fellowship for A.G.-R.), and the U.K. EPSRC and The Royal Dutch Shell plc. (I-Case award for R.B.J., EP/R511870/1) for financial support. Calculations were carried out on an in-house Odyssey HPC cluster (Cambridge) and the authors are grateful for the calculation time used.

REFERENCES

(1) Szczepura, L. F.; Witham, L. M.; Takeuchi, K. J. *Tris*(2-Pyridyl) Tripod Ligands. *Coord. Chem. Rev.* **1998**, *174* (1), 5–32.

(2) Peel, A. J.; Waters, J. E.; Plajer, A. J.; García-Rodríguez, R.; Wright, D. S. Recent Advances in the Synthesis and Application of *Tris*(Pyridyl) Ligands Containing Metallic and Semimetallic p-Block Bridgeheads. Advances in Organometallic Chemistry; Academic Press Inc., 2021; Vol. 75, pp 193−244.

(3) Bocokić, V.; Kalkan, A.; Lutz, M.; Spek, A. L.; Gryko, D. T.; Reek, J. N. H. Capsule-Controlled Selectivity of a Rhodium Hydroformylation Catalyst. *Nat. Commun.* **2013**, *4*, 1–9.

(4) Kimura, S.; Uejima, M.; Ota, W.; Sato, T.; Kusaka, S.; Matsuda, R.; Nishihara, H.; Kusamoto, T. An Open-Shell, Luminescent, Two-Dimensional Coordination Polymer with a Honeycomb Lattice and Triangular Organic Radical. *J. Am. Chem. Soc.* **2021**, *143* (11), 4329–4338.

(5) Simmonds, H. R.; Wright, D. S. Main Group Pyridyl-Based Ligands; Strategies to Mixed Metal Complexes. *Chem. Commun.* **2012**, *48* (69), 8617–8624.

(6) Zeckert, K.; Griebel, J.; Kirmse, R.; Weiß, M.; Denecke, R. Versatile Reactivity of a Lithium *Tris*(Aryl)Plumbate(II) towards Organolanthanoid Compounds: Stable Lead-Lanthanoid-Metal Bonds or Redox Processes. *Chem. Eur. J.* **2013**, *19* (24), 7718–7722.

(7) Schrader, I.; Zeckert, K.; Zahn, S. Dilithium Hexaorganostannate(IV) Compounds. *Angew. Chem. Int. Ed.* **2014**, *53* (50), 13698–13700.

(8) García-Rodríguez, R.; Hanf, S.; Bond, A. D.; Wright, D. S. A Non-Chiral Lithium Aluminate Reagent for the Determination of Enantiomeric Excess of Chiral Alcohols. *Chem. Commun.* **2017**, *53* (7), 1225–1228.

(9) Zeckert, K.; Fuhrmann, D. Bis(2-Pyridyl) and *Tris*(2-Pyridyl) Compounds of Gallium and Indium via a Redox-Transmetalation Route. *Inorg. Chem.* **2019**, *58* (24), 16736–16742.

(10) Jeong, S. Y.; Lalancette, R. A.; Lin, H.; Lupinska, P.; Shipman, P. O.; John, A.; Sheridan, J. B.; Jäkle, F. "third-Generation"-Type Functional *Tris*(2-Pyridyl)Borate Ligands and Their Transition-Metal Complexes. *Inorg. Chem.* **2016**, *55* (7), 3605–3615.

(11) Cui, C.; Lalancette, R. A.; Jäkle, F. The Elusive Tripodal *Tris*(2-Pyridyl)Borate Ligand: A Strongly Coordinating Tetraarylborate. *Chem. Commun.* **2012**, *48* (55), 6930.

(12) Morales, D.; Pérez, J.; Riera, L.; Riera, V.; Miguel, D. Molybdenum and Tungsten Tricarbonyl Complexes with the Tripodal Ligands [^{n}BuSn(2-Pyridyl)$_3$] and [RSn(Methylthiomethyl)$_3$]. *Organometallics* **2001**, *20* (22), 4517–4523.

(13) Plajer, A. J.; Crusius, D.; Jethwa, R. B.; García-Romero, Á.; Bond, A. D.; García-Rodríguez, R.; Wright, D. S. Coordination Chemistry of the Bench-Stable *Tris*-2-Pyridyl Pnictogen Ligands [E(6-Me-2-Py)$_3$] (E = As, AsO, Sb). *Dalton Trans.* **2021**, *50*, 2393–2402.

(14) Plajer, A. J.; Colebatch, A. L.; Rizzuto, F. J.; Pröhm, P.; Bond, A. D.; García-Rodríguez, R.; Wright, D. S. How Changing the Bridgehead Can Affect the Properties of Tripodal Ligands. *Angew. Chem. Int. Ed.* **2018**, *57* (22), 6648–6652.

(15) García-Romero, Á.; Plajer, A. J.; Miguel, D.; Wright, D. S.; Bond, A. D.; Álvarez, C. M.;

García-Rodríguez, R. *Tris*(2-Pyridyl) Bismuthines: Coordination Chemistry, Reactivity, and Anion-Triggered Pyridyl Coupling. *Inorg. Chem.* **2020**, *59* (10), 7103–7116.

(16) García-Romero, Á.; Martín-Álvarez, J. M.; Colebatch, A. L.; Plajer, A. J.; Miguel, D.; Álvarez, C. M.; García-Rodríguez, R. Synthesis of *Tris*(3-Pyridyl)Aluminate Ligand and Its Unexpected Stability against Hydrolysis: Revealing Cooperativity Effects in Heterobimetallic Pyridyl Aluminates. *Dalton Trans.* **2021**, *50*, 13059–13065.

(17) Yang, E. S.; Plajer, A. J.; García-Romero, Á.; Bond, A. D.; Ronson, T. K.; Álvarez, C. M.; García-Rodríguez, R.; Colebatch, A. L.; Wright, D. S. A *Tris*(3-Pyridyl)Stannane as a Building Block for Heterobimetallic Coordination Polymers and Supramolecular Cages. *Chem. Eur. J.* **2019**, *25* (61), 14003–14009.

(18) García-Romero, Á.; Martín-Álvarez, J. M.; Miguel, D.; Wright, D. S.; Álvarez, C. M.; García-Rodríguez, R. Cation- and Anion-Mediated Supramolecular Assembly of Bismuth and Antimony *Tris*(3-Pyridyl) Complexes. *Inorg. Chem.* **2021**, *60* (24), 19206–19218.

(19) Waters, J. E.; Berger, G.; Peel, A. J.; García-Rodríguez, R.; Bond, A. D.; Wright, D. S. Uncovering the Hidden Landscape of *Tris*(4-Pyridyl) Ligands: Topological Complexity Derived from the Bridgehead. *Chem. Eur. J.* **2021**, *27* (47), 12036–12040.

(20) Deshmukh, M. S.; Yadav, A.; Pant, R.; Boomishankar, R. Thermochromic and Mechanochromic Luminescence Umpolung in Isostructural Metal–Organic Frameworks Based on Cu_6I_6 Clusters. *Inorg. Chem.* **2015**, *54* (4), 1337–1345.

(21) Kumar, K. S.; Mane, V. S.; Yadav, A.; Kumbhar, A. S.; Boomishankar, R. Photochemical Hydrogen Evolution from Water by a 1D-Network of Octahedral Ni_6L_8 Cages. *Chem. Commun.* **2019**, *55* (87), 13156–13159.

(22) Deshmukh, M. S.; Mane, V. S.; Kumbhar, A. S.; Boomishankar, R. Light-Driven

Hydrogen Evolution from Water by a Tripodal Silane Based $Co^{II}_6L^1_8$ Octahedral Cage. *Inorg. Chem.* **2017**, *56* (21), 13286–13292.

(23) Waters, J. E.; Hanf, S.; Rincón-Nocito, M.; Bond, A. D.; García-Rodríguez, R.; Wright, D. S.; Colebatch, A. L. Synthesis and Coordination Behaviour of Aluminate-Based Quinolyl Ligands. *Dalton Trans.* **2021**, *50* (41), 14551–14559.

(24) Mantina, M.; Chamberlin, A. C.; Valero, R.; Cramer, C. J.; Truhlar, D. G. Consistent van Der Waals Radii for the Whole Main Group. *J. Phys. Chem. A* **2009**, *113* (19), 5806–5812.

(25) Bondi, A. Van Der Waals Volumes and Radii. *J. Phys. Chem.* **1964**, *68* (3), 441–451.

(26) Cordero, B.; Gómez, V.; Platero-Prats, A. E.; Revés, M.; Echeverría, J.; Cremades, E.; Barragán, F.; Alvarez, S. Covalent Radii Revisited. *Dalton Trans.,* **2008***,* 2832–2838.

(27) Pyykkö, P.; Atsumi, M. Molecular Single-Bond Covalent Radii for Elements 1-118. *Chem. Eur. J.* **2009**, *15* (1), 186–197.

(28) Bowmaker, G. A.; Effendy; Hart, R. D.; Kildea, J. D.; Skelton, B. W.; de Silva, E. N.; White, A. H. Lewis-Base Adducts of Group 11 Metal(I) Compounds. LXIV Syntheses, Spectroscopy and Structures of Some 1:4 Adducts of Copper(I) and Silver(I) Perchlorates with Triphenylarsine and Triphenylstibine. Aust. J. Chem. **1997**, *50* (6), 539−552.

(29) Ke, I. S.; Gabbaï, F. P. $Cu_3(\mu_2\text{-}Cl)_3$ and $Ag_3(\mu_2\text{-}Cl)_3$ Complexes Supported by Tetradentate Trisphosphino-Stibine and -Bismuthine Ligands: Structural Evidence for Triply Bridging Heavy Pnictines. *Aust. J. Chem.* **2013**, *66* (10), 1281–1287.

(30) Scudder, M.; Dance, I. Dimorphic Intra- and Intermolecular Aryl Motifs in Symmetrical Hexafaceted Molecules $(Ar_nX)_3Y\text{-}Z\text{-}Y(XAr_n)_3$. *Chem. Eur. J.* **2002**, *8* (23), 5456–5468.

(31) Shannon, R. D. Revised Effective Ionic Radii and Systematic Studies of Interatomie

Distances in Halides and Chaleogenides. *Acta Cryst.* **1976**, *A32*, 751–767.

(32) Hanf, S.; Colebatch, A. L.; Stehr, P.; García-Rodríguez, R.; Hey-Hawkins, E.; Wright, D. S. An Experimental and Theoretical Study of the Coordination and Donor Properties of *Tris*-2-Pyridyl-Phosphine Ligands. *Dalton Trans.* **2020**, *49* (16), 5312–5322.

(33) Cingolani, A.; Hanna, J. V; Pellei, M.; Pettinari, C.; Santini, C.; Skelton, B. W.; White, A. H.; Chimiche, S.; Uni, V.; Agostino, V. S.; Mc, C.; Kimia, J.; Uni, F.; Negeri, V.; Surabaya, J. Crystal Structures and Vibrational and Solution and Solid-State (CPMAS) NMR Spectroscopic Studies in Triphenyl Phosphine , Arsine , and Stibine Silver (I) Bromate Systems , ($R_3E)_xAgBrO_3$ (E = P, As ,Sb ; x = 1-4). I*norg. Chem.* **2003**, *42* (16) 4938–4948.

(34) Li, Y.-Z.; Gonguly, R.; Hong, K. Y.; Li, Y.; Tessensohn, M. E.; Webster, R.; Leong, W. K. Stibine-protected Au_{13} nanoclusters: syntheses, properties and facile conversion to GSH-protected Au_{25} nanocluster *Chem. Sci.*, **2018**, *9*, 8723-8730.

(35) Fernández, E. J.; Laguna, A.; López-De-Luzuriaga, J. M.; Monge, M.; Nema, M.; Olmos, M. E.; Pérez, J.; Silvestru, C. Experimental and Theoretical Evidence of the First Au(I)···Bi(III) Interaction. *Chem. Commun.* **2007**, *28* (6), 571–573.

(36) Kořenková, M.; Kremláček, V.; Erben, M.: Jirásko, R.; Proft, F. D.; Turek, J.; Jambor, R.; Růžička, A.; Císařová, I.; Dostál, L. Heavier Pnictinidene Gold(I) Complexes. *Dalton Trans.*, **2018**, *47*, 14503-14514.

(37) Lin, T. P.; Ke, I. S.; Gabbaï, F. P. σ-Accepting Properties of a Chlorobismuthine Ligand. *Angew. Chem. Int. Ed.* **2012**, *51* (20), 4985–4988.

(38) Ke, I. S.; Gabbaï, F. P. σ-Donor/Acceptor-Confused Ligands: The Case of a Chlorostibine. *Inorg. Chem.* **2013**, *52* (12), 7145–7151.

(39) Tschersich, C.; Braun, B.; Herwig, C.; Limberg, C. Coordination of Noble Metals by an Ambiphilic PBiP Pincer Ligand: Metallophilic Bi-Cu and Bi-Ag Interactions. *J. Organomet. Chem.* **2015**, *784*, 62–68.

(40) Smith, J. E.; Yang, H.; Gabbaï, F. P. An Electrophilic, Intramolecularly Base-Stabilized Platinum-Antimony Complex. *Organometallics* **2021**, *40* (23), 3886–3892.

(41) Frisch, M. J.; Trucks, G. W.; Schlegel, H. B.; Scuseria, G. E.; Robb, M. A.; Cheeseman, J. R.; Scalmani, G.; Barone, V.; Petersson, G. A.; Nakatsuji, H.; Li, X.; Caricato, M.; Marenich, A. V.; Bloino, J.; Janesko, B. G.; Gomperts, R.; Mennucci, B.; Hratchian, H. P.; Ortiz, J. V.; Izmaylov, A. F.; Sonnenberg, J. L.; Williams-Young, D.; Ding, F.; Lipparini, F.; Egidi, F.; Goings, J.; Peng, B.; Petrone, A.; Henderson, T.; Ranasinghe, D.; Zakrzewski, V. G.; Gao, J.; Rega, N.; Zheng, G.; Liang, W.; Hada, M.; Ehara, M.; Toyota, K.; Fukuda, R.; Hasegawa, J.; Ishida, M.; Nakajima, T.; Honda, Y.; Kitao, O.; Nakai, H.; Vreven, T.; Throssell, K.; Montgomery, J. A., Jr.; Peralta, J. E.; Ogliaro, F.; Bearpark, M. J.; Heyd, J. J.; Brothers, E. N.; Kudin, K. N.; Staroverov, V. N.; Keith, T. A.; Kobayashi, R.; Normand, J.; Raghavachari, K.; Rendell, A. P.; Burant, J. C.; Iyengar, S. S.; Tomasi, J.; Cossi, M.; Millam, J. M.; Klene, M.; Adamo, C.; Cammi, R.; Ochterski, J. W.; Martin, R. L.; Morokuma, K.; Farkas, O.; Foresman, J. B.; Fox, D. J. Gaussian 16, revision C.01; Gaussian, Inc.: Wallingford, CT, **2019**.

(42) Austin, A.; Petersson, G. A.; Frisch, M. J.; Dobek, F. J.; Scalmani, G.; Throssell, K. A Density Functional with Spherical Atom Dispersion Terms. *J. Chem. Theory Comput.* **2012**, *8*, 4989−5007.

(43) Figgen, D.; Rauhut, G.; Dolg, M.; Stoll, H. Energy-Consistent Pseudopotentials for Group 11 and 12 Atoms: Adjustment to Multi-Configuration Dirac−Hartree−Fock Data. *Chem.*

Phys. **2005**, *311*, 227−244.

(44) Metz, B.; Stoll, H.; Dolg, M. Small-core multiconfiguration-Dirac−Hartree−Fock-Adjusted Pseudopotentials for Post- d Main Group Elements: Application to PbH and PbO. *J. Chem. Phys.* **2000**, *113* (7), 2563−2569.

(45) Peterson, K. A. Systematically Convergent Basis Sets with Relativistic Pseudopotentials. I. Correlation Consistent Basis Sets for the Post-d Group 13-15 Elements. *J. Chem. Phys.* **2003**, *119* (21), 11099–11112.

(46) Peterson, K. A.; Puzzarini, C. Systematically Convergent Basis Sets for Transition Metals. II. Pseudopotential-Based Correlation Consistent Basis Sets for the Group 11 (Cu, Ag, Au) and 12 (Zn, Cd, Hg) Elements. *Theor. Chem. Acc.* **2005**, *114*, 283−296.

(47) Pritchard, B. P.; Altarawy, D.; Didier, B.; Gibson, T. D.; Windus, T. L. New Basis Set Exchange: An Open, Up-to-Date Resource for the Molecular Sciences Community. *J. Chem. Inf. Model.* **2019**, *59* (11), 4814–4820.

(48) Feller, D. Computational Chemistry Calculations. *J. Comput. Chem.* **1996**, *17* (13), 1571–1586.

(49) Schuchardt, K. L.; Didier, B. T.; Elsethagen, T.; Sun, L.; Gurumoorthi, V.; Chase, J.; Li, J.; Windus, T. L. Basis Set Exchange: A Community Database for Computational Sciences. *J. Chem. Inf. Model.* **2007**, *47* (3), 1045–1052.

(50) Dennington, R.; Keith, T. A.; Millam, J. M. GaussView, version 6.1; Semichem Inc.: Shawnee Mission, KS, **2016**.

(51) Glendening, E. D.; Badenhoop, J. K.; Reed, A. E.; Carpenter, J. E.; Bohmann, J. A.; Morales, C. M.; Karafiloglou, P.; Landis, C. R.; Weinhold, F. NBO 7.0; Theoretical Chemistry Institute, University of Wisconsin: Madison, WI, 2018.

SYNOPSIS

Tris(quinolyl) ligands E(2-Me-8-qy)$_3$ [E = Sb(**1**) and Bi(**2**)] can adopt a greater range of coordination modes than their *tris*(2-pyridyl) counterparts. In the antimony-based ligand **1**, the donor N-atoms and the lone-pair on the bridgehead atom can coordinate a single metal ion simultaneously. The lower Lewis basicity of the Bi center in **2** and the greater polarity of the Bi-C bonds result in a switch in the coordination mode to an unusual *N,N,(π-)C*-mode as well as non-innocent reactivity.